# Analysis of Crucial End Effects of Switched Reluctance Machines by 3D Finite Element Calculations

C. Grabner

Research and Development Motors, Siemens AG
Siemensstrasse 15, D-97616 Bad Neustadt an der Saale (Germany)
phone: +49 9771 952366, fax: +49 9771 954063, e-mail: **grabner.christian@siemens.com**

**Abstract.** The dynamic behavior of switched reluctance machines is mainly governed by the stator leakage inductance. A comparison of machine parameters, such as e.g. the ratio between self and leakage inductance, for constructions based on two different axial lengths is suitable for a deeper knowledge about the influence of the nonlinear iron saturation effects within higher electrical currents. Therefore, 3D nonlinear numerical field calculations are carried out to in order to obtain the self and leakage inductances from a magnetic energy approach.

**Key Words.** Finite element analysis, Switched reluctance machine, Homogenization technique, Self and leakage inductance.

## 1. Introduction

Nonlinear 3D numerical field calculations are carried out in order to determine the self and stray inductances and their saturation dependency in a most accurate and fast way [1,2]. Some important characteristics of the concerned switched reluctance machines are summarized in Table I.

Arising modeling problems due to the laminated iron stator sheets and the very thin insulation layers are treated in the numerical investigation by means of a special homogenization technique. Thus, the complex anisotropic iron structure along the axial machine length could be included in the finite element calculation in a very efficient way.

TABLE I - Main characteristics of both 6/4 machines

| | | |
|---|---|---|
| Electrical stator phase current | 0…5 | A |
| Rated voltage of the axial short machine | 30 | V |
| Rated voltage of the axial long machine | 55 | V |
| Number of stator windings | 3 | |
| Airgap distance | 0.5 | mm |
| Inner stator diameter | 58.0 | mm |
| Iron length of the axial short machine | 31.0 | mm |
| Iron length of the axial long machine | 63.0 | mm |

The uniqueness of the numerical calculated field solution is established with the aid of a gauged magnetic vector potential formulation, whereby nodal shape functions of higher order are utilized. The performed numerical evaluation of the self and leakage inductances is based on a general energy approach.

The separate integration of field quantities, which are directly accessible from the nodal solutions, over volumes enclosing even the complete iron and airgap domains or the stray field air regions, delivers the required self and leakage inductances, respectively. Hence, local occurring nonlinear iron saturation effects are regarded correctly.

## 2. Finite Element Formulation for 3D Nonlinear and Anisotropic Problems

The consideration of higher order nodal functions enforces the incorporation of a gauged magnetic vector potential in order to avoid numerical difficulties due to a serious ill-conditioning [3]. Thus, the gauging ensures numerical stability. Unfortunately, some adverse effects on the satisfaction of the interface conditions along air and iron are occurring due to nodal element formulations [4]. However, the usage of a homogenization technique for the non-homogeneous structure of the laminated stator inherently avoids those inaccuracies of the used numerical algorithm.

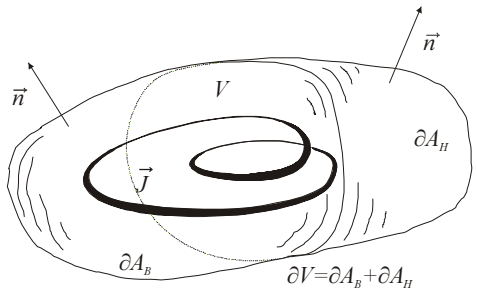


Fig. 1. Volume with enclosed outer boundary surface $\partial V=\partial A_B+\partial A_H$ and arbitrary current density distributions inside.

The local magnetic field distribution inside the volume of Fig.1 can be obtained with the aid of the gauged magnetic vector potential

$$\vec{\nabla}\cdot\vec{A}=0\ , \qquad \vec{\nabla}\times\vec{A}=\vec{B}\ , \tag{1}$$

from the unique relationship

$$\vec{\nabla}\times\left(\underset{\sim}{\upsilon}\cdot\vec{\nabla}\times\vec{A}\right)-\vec{\nabla}\left(\upsilon_0\,\vec{\nabla}\cdot\vec{A}\right)=\vec{J}\ , \tag{2}$$

whereby $\upsilon_0$ denotes the reluctivity of the air [5,6].

The continuum field conditions on the boundary part $\partial A_B$ of Fig.1 are given with

$$\left(\upsilon_0\,\vec{\nabla}\cdot\vec{A}\right)=0\ , \tag{3}$$

$$\vec{n}\times\vec{A}=0\ , \tag{4}$$

and those on the boundary section $\partial A_H$ are established by

$$\vec{n}\times\left(\underset{\sim}{\upsilon}\cdot\vec{\nabla}\times\vec{A}\right)=0\ , \tag{5}$$

$$\vec{n}\cdot\vec{A}=0\ . \tag{6}$$

Thereby, the normal unit vector $\vec{n}$ at the surfaces $\partial A_B$ and $\partial A_H$ in Fig.1 is used.

Moreover, the constitutive nonlinear material relationship

$$\vec{H}=\underset{\sim}{\upsilon}\left(B\right)\cdot\vec{B}\ , \tag{7}$$

is introduced in (2), whereby the permeability tensor

$$\underset{\sim}{\upsilon}\left(B\right)=\upsilon_{xx}\left(B\right)\vec{e}_x\otimes\vec{e}_x+\upsilon_{yy}\left(B\right)\vec{e}_y\otimes\vec{e}_y+\upsilon_{zz}\left(B\right)\vec{e}_z\otimes\vec{e}_z \tag{8}$$

is defined in reference to the arrangement depicted in Fig.2.

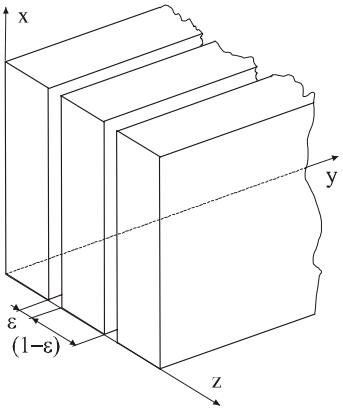


Fig. 2. Arrangement of the axial laminated adjoining iron structure.

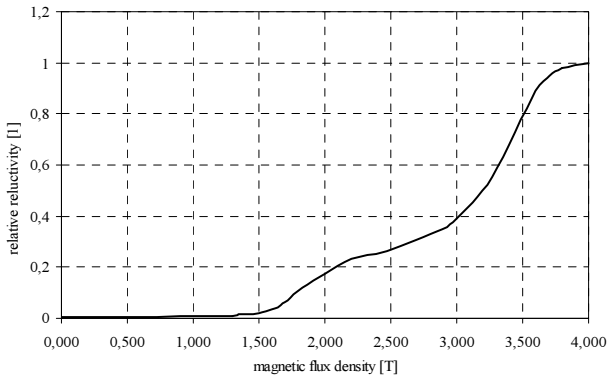


Fig.3. Relative reluctivity $\hat{\upsilon}_{xx}$ in dependency of the magnetic flux density for one primary single iron sheet.

The iron stator laminations are very thin and closely packed in comparison to the other machine dimensions. Thus, the proposed implementation takes account of a strongly anisotropic macroscopic reluctivity tensor (8) with the proposed averaged components

$$\upsilon_{xx}\left(B\right)=\upsilon_{yy}\left(B\right)=\frac{1}{\frac{(1-\varepsilon)}{\hat{\upsilon}_{xx}(B)}+\frac{\varepsilon}{\upsilon_0}}\ ,\quad \upsilon_{zz}\left(B\right)=\left(1-\varepsilon\right)\hat{\upsilon}_{xx}\left(B\right)+\varepsilon\upsilon_0 \tag{9}$$

The local interaction of each laminated sheet, which is usually characterized by the nonlinear iron reluctivity $\hat{\upsilon}_{xx}\left(B\right)$ depicted in Fig.3, with the insulation thickness $\varepsilon=0.0003\,\mathrm{m}$ is regarded in the numerical field calculation by the homogenization technique (9) [7,8].

The performed numerical approximation of the primary unknown potential (1) over the considered domain is based on the finite element mesh depicted in Fig.4.

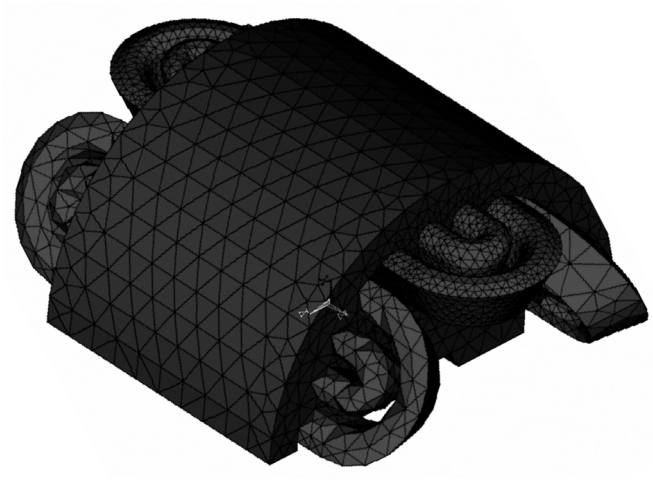

Fig.4. Finite element discretization of the switched reluctance machine.

The potentials are thereby expanded in terms of isoparametric shape functions of higher order which are associated with the obtained nodal results of the established mesh. Thereby, the performed computation uses two subsets of nodal numbers. Specific nodes $j=\left(n+1\right)\ldots n_{node}$ are laying on boundaries which have to fulfill the well known Dirichlet conditions, whereas all other nodal values $j=1\ldots n$ are unknown. The maximal number of used nodes is denoted by $n_{node}$.

The nodal approximation of the gauged magnetic vector potential is performed in a global Cartesian coordinate system $\left(x,y,z\right)$ with

$$\vec{A}\approx\vec{A}_n=\vec{A}_D+\sum_{j=1}^{n}N_j\left(x,y,z\right)\vec{\alpha}_j\ , \tag{10}$$

whereby the unknown nodal values

$$\vec{\alpha}_j=\alpha_{xj}\,\vec{e}_x+\alpha_{yj}\,\vec{e}_y+\alpha_{zj}\,\vec{e}_z \tag{11}$$

are introduced at each node $j$ [9,10].

The shape functions $N_j(x,y,z)$ associated with node $j$ assume

$$N_j(x,y,z)=\begin{cases}1 & \text{node } j\\ 0 & \text{else}\end{cases} \tag{12}$$

the value one at this node and the value zero at any other nodes. The additionally defined nodal boundary contribution

$$\vec{A}_D=\sum_{j=n+1}^{n_{node}} N_j(x,y,z)\,\vec{\beta}_j \tag{13}$$

is given at all nodes $j=(n+1)\ldots n_{node}$ by default nodal values $\vec{\beta}_j$.

Furthermore, the known electrical current density is approximated by

$$\vec{J}\approx\vec{J}_n=\vec{J}_D=\sum_{l=1}^{n_{node}} N_l(x,y,z)\,\vec{\gamma}_l \tag{14}$$

with the aid of given nodal values $\vec{\gamma}_l$ [11]. Further anisotropic material properties are assumed as [11]

$$\underset{\sim}{\upsilon}_n(B_n)=\sum_{l=1}^{n_{node}} N_l(x,y,z)\,\underset{\sim}{\upsilon}_l(B_n)\ . \tag{15}$$

The derived numerical solution of the established boundary problem is based on the usual Galerkin technique in addition to the proposed finite element approach [12,13]. Thereby, the governing field equation (2) inside the investigated volume of the switched reluctance machine is approximated by (10). Unfortunately, a residual remains due to the insufficient approximation (10). By means of Galerkin, this residual is additionnally weighted by the shape functions (12). The solutions method is based on vanishing of this weighted residual over the domain under consideration.

The governing Galerkin relation and the approximately fulfilled Neumann boundary conditions (3),(5) are rewritten with two introduced space dependent Dirac functions $\delta_{\partial A_H}$ and $\delta_{\partial A_B}$, defined at the boundaries $\partial A_H$ and $\partial A_B$, respectively, as [3]

$$\begin{aligned}&\int_V N_i\Big\{\vec{\nabla}\times\Big(\underset{\sim}{\upsilon}_n\cdot\vec{\nabla}\times\vec{A}_n\Big)-\vec{\nabla}\Big(\upsilon_0\,\vec{\nabla}\cdot\vec{A}_n\Big)+\\&+\delta_{\partial A_H}\Big[\vec{n}\times\Big(\underset{\sim}{\upsilon}_n\cdot\vec{\nabla}\times\vec{A}_n\Big)\Big]+\delta_{\partial A_B}\Big[\vec{n}\Big(\upsilon_0\,\vec{\nabla}\cdot\vec{A}_n\Big)\Big]\Big\}\,\mathrm{d}V=\\&=\int_V N_i\vec{J}_n\,\mathrm{d}V\ .\end{aligned} \tag{16}$$

The necessary Dirichlet boundary conditions (4) on $\partial A_B$ and (6) on $\partial A_H$ must be fulfilled by (10) for all nodes which are located in the section $\partial A_B$ according to

$$\vec{n}\times\vec{A}_D=0\ ,\quad \vec{n}\times\Big(N_j(x,y,z)\,\vec{\alpha}_j\Big)=\vec{0}\ , \tag{17}$$

which is implicitly given due to the chosen node numbering and the properties (12).

In the same manner, the condition (6) on the section $\partial A_H$ is fulfilled with

$$\vec{n}\cdot\vec{A}_D=0\ ,\quad \vec{n}\cdot\Big(N_j(x,y,z)\,\vec{\alpha}_j\Big)=0\ . \tag{18}$$

Partial integration of (16) leads with (17),(18) to the practicable relation [11]

$$\int_V\Big[\vec{\nabla}N_i\times\Big(\underset{\sim}{\upsilon}_n\cdot\vec{\nabla}\times\vec{A}_n\Big)-\vec{\nabla}N_i\Big(\upsilon_0\,\vec{\nabla}\cdot\vec{A}_n\Big)\Big]\,\mathrm{d}V=-\int_V N_i\cdot\vec{J}_n\,\mathrm{d}V \tag{19}$$

Thus, the magnetic field distribution is completely described by a nodal magnetic vector potential formulation. The unknown coefficients $\vec{\alpha}_j$ in (10) are calculated from the nonlinear relationship (19) by applying (10),(14),(15).

## 3. Computation of Nonlinear Inductances from a Magnetic Energy Principle

The total magnetic energy inside the closed volume of Fig.1 can be approached from [14]

$$W=\int_V\vec{H}\cdot\vec{B}\,\mathrm{d}V\ . \tag{20}$$

A rewritten form of (20) based on the magnetic vector potential formulation and the boundary conditions (4) and (5) yields

$$W=\int_V\vec{A}\cdot\Big[\vec{\nabla}\times\Big(\underset{\sim}{\upsilon}\cdot\vec{\nabla}\times\vec{A}\Big)\Big]\,\mathrm{d}V\ . \tag{21}$$

The nonlinear common flux linkage and the electrical current is usually coupled as

$$W=I\,\Phi\ , \tag{22}$$

whereby the introduced splitting of the common flux linkage

$$\Phi=L(I)\,I \tag{23}$$

is mainly nonlinear in case of surrounding iron materials. The expression (23) stands for the total magnetic flux linkage, which is produced by the current carrying regions situated in the considered domain shown in Fig.4.

Consequently, different nonlinear inductances are generally derived from (21),(22),(23) by applying (10), (13),(15) for the arrangement in Fig.4 according to

$$\begin{aligned}L(I)=\frac{1}{I^2}\int_V&\Big\{\sum_{j=n+1}^{n_{node}}N_j\vec{\beta}_j+\sum_{j=1}^{n}N_j\vec{\alpha}_j\Big\}\cdot\\&\cdot\Big\{\vec{\nabla}\times\Big[\sum_{l=1}^{n_{node}}N_l\underset{\sim}{\upsilon}_l\cdot\Big(\sum_{j=n+1}^{n_{node}}\vec{\nabla}N_j\times\vec{\beta}_j+\sum_{j=1}^{n}\vec{\nabla}N_j\times\vec{\alpha}_j\Big)\Big]\Big\}\mathrm{d}V\end{aligned} \tag{24}$$

The self inductance is obtained from (24) by extending the integral over domains of Fig.4, which are including the complete homogenized iron structure, conductors as well as all air volumes between rotor and stator part. The relation (24) will be evaluated over relevant air and conducting domains of Fig.4, which are lying in the stray field end regions outside the homogenized stator part in order to obtain the end leakage inductance.

## 4. Comparison of Nonlinear Self Inductances in the "Aligned" Rotor Position

Several 3D numerical field calculations are carried out for the "aligned" rotor position by a stepwise increased electrical current density (14) in one stator phase winding of Fig.4. The obtained results of the self and leakage inductances (24) are compared in Table II with regard to the crucial effect of the different axial machine length. Thereby the main focus is put on the ratio of self inductance versus the leakage values as well as the common stator inductance of both constructions.

A significant dependency of the obtained self inductances on local occurring nonlinear magnetic saturation effects can be seen from Table II. In both investigated types, the self inductances decrease from maximal values at lowest currents to approximately 62% within a maximal electrical current of 5A. The reduction of the end leakage inductance is given from Table II with nearby 76% and 77% for the "short" and "long" machine, respectively.

The ratio between the end leakage and the self inductance in Table II increases within higher currents about 121% in case of the "short" machine and approximately about 124% in case of the "long" machine. But a comparison of the reactance ratios between both types shows distinctively that the ratio of the "longer" machine is almost less than half of the "shorter" machine. Moreover, both ratios are independent of any injected current.

TABLE II - "Aligned" inductances of the "Short" (Index S) and the "Long" (Index L) 6/4 machine

| $I_S$ | [A] | 1 | 2 | 3 | 4 | 5 |
|---|---|---|---|---|---|---|
| $L_{d\sigma S}$ | [mH] | 1.04 | 1.02 | 0.91 | 0.83 | 0.79 |
| $L_{d S}$ | [mH] | 20.00 | 19.25 | 16.29 | 14.23 | 12.57 |
| $L_{d\sigma S}/L_{d S}$ | [%] | 5.22 | 5.32 | 5.61 | 5.87 | 6.32 |
| $L_{d.S}$ | [mH] | 21.04 | 20.27 | 17.20 | 15.06 | 13.36 |
| $I_L$ | [A] | 1 | 2 | 3 | 4 | 5 |
| $L_{d\sigma L}$ | [mH] | 1.02 | 1.01 | 0.91 | 0.83 | 0.79 |
| $L_{d L}$ | [mH] | 40.03 | 39.78 | 34.39 | 28.46 | 25.14 |
| $L_{d\sigma L}/L_{d L}$ | [%] | 2.54 | 2.57 | 2.64 | 2.92 | 3.15 |
| $L_{d.L}$ | [mH] | 41.05 | 40.79 | 35.30 | 29.299 | 25.93 |

## 5. Comparison of Nonlinear Self Inductances in the "Unaligned" Rotor Position

Numerical results concerning the self and leakage inductances for the "unaligned" rotor position are comparatively listed in Table III for both investigated machines. Moreover, the ratio of self and leakage value and the total inductance are included for each case.

Reduced magnetic saturation effects within the "unaligned" position are obvious in Table III due to a stepwise increased electrical current density excitation (14). The self and end leakage inductances have only a small declining dependence on the stator current excitations. The self inductance decreases about 99.6% and 99.4% in case of the "short" and the "long" machine, respectively. Furthermore, the reduction of the end leakage inductance can be approximated by 98.9% and 98.6% for both machine types.

The ratio of the end leakage and self inductance in Table III decreases within higher currents about 0.7% in case of the "short" machine and approximately about 0.8% in case of the "long" construction. Table III shows imposingly, that the ratio of the "short" machine is always twice than the that of the "long" machine and again independent of any current.

TABLE III - "Unaligned" inductances of the "Short" (Index S) and the "Long" (Index L) 6/4 machine

| $I_S$ | [A] | 1 | 2 | 3 | 4 | 5 |
|---|---|---|---|---|---|---|
| $L_{d\sigma S}$ | [mH] | 0.904 | 0.902 | 0.900 | 0.899 | 0.894 |
| $L_{d S}$ | [mH] | 4.044 | 4.040 | 4.039 | 4.035 | 4.028 |
| $L_{d\sigma S}/L_{d S}$ | [%] | 22.35 | 22.33 | 22.28 | 22.28 | 22.19 |
| $L_{d.S}$ | [mH] | 4.948 | 4.942 | 4.939 | 4.934 | 4.922 |
| $I_L$ | [A] | 1 | 2 | 3 | 4 | 5 |
| $L_{d\sigma L}$ | [mH] | 0.906 | 0.905 | 0.903 | 0.900 | 0.893 |
| $L_{d L}$ | [mH] | 8.082 | 8.078 | 8.062 | 8.052 | 8.030 |
| $L_{d\sigma L}/L_{d L}$ | [%] | 11.21 | 11.20 | 11.20 | 11.17 | 11.12 |
| $L_{d.L}$ | [mH] | 8.988 | 8.983 | 8.966 | 8.954 | 8.930 |

## 6. Conclusion

The space dependent nonlinear inductances of two different switched reluctance machine designs are derived from a numerical vector potential formulation and the application of the magnetic energy principle.

Modeling problems arising in the finite element calculation due to the laminated iron stator sheets and the very thin insulation layers are overcome by the utilization of a novel homogenization technique.

## References


[1] K. Hameyer, R. Belmans, Numerical Modeling and Design of Electrical Machines and Devices, WIT Press, 1999, Southampton.

[2] S. Ratnajeevan, H. Hoole, Computer Aided Analysis and Design of Electromagnetic Devices, Elsevier, 1989, Amsterdam.

[3] O. Biro, K. Preis, K. R. Richter, *On the Use of the Magnetic Vector Potential in the Nodal and Edge Finite Element Analysis of 3D Magnetostatic Problems*, IEEE Transactions on Magnetics. Vol. 32, No. 5, 1996.

[4] K. Preis, I. Bardi, O. Biro, C. Magele, G. Vrisk, K.R. Richter, *Different Finite Element Formulations of 3D Magnetostatic Fields*, IEEE Transactions on Magnetics. Vol. 28, No. 2, 1992.

[5] K. Preis, I. Bardi, O. Biro, C. Magele, W. Renhard, K.R. Richter, G. Vrisk, *Numerical Analysis of 3D Magnetostatic Fields*, IEEE Transactions on Magnetics. Vol. 27, No. 5, 1991.

[6] C. Magele, H. Stögner, K. Preis, *Comparison of Different Finite Element Formulations for 3D Magnetostatic Problems*, IEEE Transactions on Magnetics. Vol. 32, No. 5, 1996.

[7] K.J. Bins, P.J. Lawrenson, C.W. Trowbridge, The Analytical and Numerical Solution of Electric and Magnetic Fields, John Wiley & Sons, 1992, Chichester.

[8] A. de Rochebrune, J.M. Dedulle, J.C. Sabonnadiere, *A Technique of Homogenization Applied to the Modeling of Transformers*, IEEE Transactions on Magnetics. Vol. 26, No. 2, 1990.

[9] A. Kost, Numerische Methoden in der Berechnung Elektromagnetischer Felder, Springer Verlag, 1994, Berlin Heidelberg.

[10] O.C. Zienkiewicz, R.L. Taylor, The Finite Element Method, Butterworth Heinemann, 2000, Oxford.

[11] H. Stögner, Anwendung der Methode der Finiten Elemente zur Numerischen Berechnung Dreidimensionaler Elektromagnetischer Felder, Habilitationsschrift, 1987, Graz.

[12] R. Schwarz, Methode der Finiten Elemente, B. G. Teubner, 1984, Stuttgart.

[13] K.J. Bathe, Finite Element Procedures, Prentice Hall, 1996, New Jersey.

[14] R.M. Fano, J.J. Chu, R.B. Adler, Electromagnetic Fields, Energy and Forces, John Wiley & Sons, 1960, London.